

ALWNN Empowered Automatic Modulation Classification: Conquering Complexity and Scarce Sample Conditions

Yunhao Quan*, Chuang Gao[†], Nan Cheng*, Zhijie Zhang*, Zhisheng Yin*, Wenchao Xu*, and Danyang Wang*

*School of Telecommunications Engineering, Xidian University, Xi'an, China

[†]CSSC International Engineering Co., Ltd., Beijing 100121, China;

Email: {qyh, xcwang_1}@stu.xidian.edu.cn; {zsyin, dywang}@xidian.edu.cn
; dr.nan.cheng@ieee.org; gaochuang@csic602.com.cn

Abstract—In Automatic Modulation Classification (AMC), deep learning methods have shown remarkable performance, offering significant advantages over traditional approaches and demonstrating their vast potential. Nevertheless, notable drawbacks, particularly in their high demands for storage, computational resources, and large-scale labeled data, which limit their practical application in real-world scenarios. To tackle this issue, this paper innovatively proposes an automatic modulation classification model based on the Adaptive Lightweight Wavelet Neural Network (ALWNN) and the few-shot framework (MALWNN). The ALWNN model, by integrating the adaptive wavelet neural network and depth separable convolution, reduces the number of model parameters and computational complexity. The MALWNN framework, using ALWNN as an encoder and incorporating prototype network technology, decreases the model's dependence on the quantity of samples. Simulation results indicate that this model performs remarkably well on mainstream datasets. Moreover, in terms of Floating Point Operations Per Second (FLOPS) and Normalized Multiply - Accumulate Complexity (NMACC), ALWNN significantly reduces computational complexity compared to existing methods. This is further validated by real-world system tests on USRP and Raspberry Pi platforms. Experiments with MALWNN show its superior performance in few-shot learning scenarios compared to other algorithms.

Index Terms—Adaptive Lightweight Wavelet Neural Network, Automatic Modulation Classification, Depthwise Separable Convolutions.

I. INTRODUCTION

The rapid evolution of modern wireless communication technologies has led to increasingly sophisticated modulation schemes in wireless channels [1], while burgeoning user demands and exponential growth in data transmission have created congested electromagnetic environments that intensify spectrum scarcity [2]. This paradigm shift necessitates robust automatic modulation classification (AMC) solutions capable of rapidly identifying signal modulation types without prior transmitter knowledge. As an indispensable bridge between signal detection and demodulation, AMC plays a vital role in both civilian and military applications including cognitive radio networks, electronic warfare systems, adaptive modulation architectures, and spectrum monitoring infrastructures. The critical need for efficient AMC implementations stems from their fundamental position in enabling intelligent signal processing across next-generation communication ecosystems.

Conventional AMC approaches are systematically categorized into two principal paradigms: likelihood-based (LB) [3] and feature-based (FB) [4] methodologies. The LB framework

formulates AMC as a hypothesis testing problem through Bayesian estimation derived from signal likelihood functions, yet demonstrates critical constraints including susceptibility to channel impairments such as frequency offsets and multipath fading, prohibitive computational complexity causing impractical latency exceeding one second per classification, and fundamental incompatibility with real-time processing requirements. In contrast, FB techniques employ a dual-stage architecture comprising expert-designed feature extraction followed by machine learning classification. The feature extraction stage focuses on deriving instantaneous characteristics such as phase variations combined with statistical descriptors including higher-order cumulants, while the classification phase utilizes models ranging from decision trees to neural networks. However, conventional LB/FB methods exhibit operational limitations through rigid feature engineering that impedes adaptation to dynamic channel conditions, substantial dependence on domain-specific prior knowledge, and sub-optimal efficiency in evolving electromagnetic environments. This technical landscape necessitates next-generation AMC solutions capable of balancing computational efficiency with environmental adaptability while maintaining classification fidelity.

Deep learning (DL), with its hierarchical feature extraction capabilities and data-driven learning paradigm, has become fundamental in addressing AMC challenges. Unlike conventional approaches requiring prior knowledge of transmission parameters, DL-based methods autonomously learn discriminative patterns directly from raw signal representations. O'Shea *et al.* [5] pioneered the application of convolutional neural networks (CNNs) to AMC, demonstrating superior performance over handcrafted-feature methods through end-to-end learning from time-domain in-phase/quadrature (IQ) samples. Subsequently, Meng *et al.* [6] enhanced CNN robustness via a dual-phase training strategy incorporating transfer learning. Nevertheless, these CNN-centric approaches primarily exploit localized spatial features while disregarding temporal dependencies in signal sequences. To comprehensively model spatiotemporal characteristics, West *et al.* [7] developed the convolutional long short-term deep neural network (CLDNN), synergistically integrating recurrent neural networks (RNNs) with CNNs. Further advancing this architecture, Xu *et al.* [8] proposed the multi-channel CLDNN (MC-LDNN), which augments spatial feature extraction through parallelized con-

volutional pathways.

While DL-based AMC demonstrates promising capabilities, two domain-specific barriers hinder practical deployment [9]. First, dynamic spectrum sharing disrupts signal statistical regularity, adversarial interference obscures modulation fingerprints, and time-varying channels invalidate static training assumptions [10]. These interacting phenomena create compounded data reliability challenges under embedded platform constraints. Second, inherent architectural complexity of DL-based AMC methods induces computational overload incompatible with resource-constrained edge devices [11], causing prohibitive latency and power consumption for real-time systems [12]. This dual exigency demands lightweight learning frameworks that synergistically address environmental uncertainty and hardware efficiency through computational paradigm innovation while preserving classification robustness [13].

This paper proposes ALWNN, a lightweight neural network for AMC that integrates adaptive wavelet transformations and depthwise separable convolutions. The architecture achieves multi-level feature extraction while reducing computational complexity and parameter count by one to two orders of magnitude. For few-shot scenarios, we introduce MALWNN, a prototype network-based framework leveraging ALWNN as its encoder, which exhibits superior data efficiency compared to existing methods. Practical deployments on USRP platforms and Raspberry Pi 4B systems validate the framework's effectiveness. The main contributions of this paper are summarized as follows.

- 1) A lightweight model architecture is proposed for efficient and accurate signal modulation classification, incorporating depthwise separable convolutions to reduce model complexity and enhance computational efficiency.
- 2) To overcome the dependence of traditional DL methods on a large amount of labeled data, MALWNN is proposed to enhance the performance of the model under the condition of small-sample labeled data.
- 3) The AWLNN architecture achieved superior performance on benchmark datasets, maintaining comparable accuracy to conventional methods while reducing parameters and computational complexity by 1-2 orders of magnitude. Hardware implementations on USRP and Raspberry Pi 4B platforms further verified these efficiency improvements.
- 4) A large number of evaluations based on the RadioML2018.01a dataset for the proposed MALWNN framework have shown that MALWNN achieves better accuracy than existing methods under a small number of samples.

The remainder of this paper is organized as follows. The related work is introduced in Section II. In Section III, we introduce the system model and conduct problem simulations. In Section IV, the proposed ALWNN model and MALWNN architecture will be introduced. In Section V, the performance of the proposed ALWNN algorithm and MALWNN framework

is evaluated through extensive simulation experiments. Subsequently, in Section VI, the actual performance of the models is evaluated using USRP and Raspberry Pi. We conclude the full paper in Section VII.

II. RELATED WORKS

In recent years, numerous lightweight AMC methodologies have been developed, encompassing technical directions such as lightweight architectural design, model compression, and knowledge distillation, with the objective of enhancing modulation recognition efficiency on resource-constrained edge devices. To address practical scenarios with limited training samples, novel AMC approaches based on weakly-supervised learning paradigms have been proposed. The following sections provide a systematic analysis of these technical approaches.

A. Structural Design-based Methods

Structural design methodologies for lightweight AMC focus on developing efficient network architectures to reduce computational demands [14], [15]. A prevalent strategy involves replacing standard convolutional layers with depthwise separable convolutions, significantly decreasing parameter counts while preserving feature extraction capabilities. Further complexity reduction can be achieved through low-rank decomposition techniques, which approximate convolutional weight matrices via products of lower-dimensional factors. Complementing these manual design approaches, Neural Architecture Search (NAS) employs reinforcement learning or evolutionary algorithms to automatically discover optimal network structures [16], [17]. This automated paradigm systematically explores architectural tradeoffs between classification accuracy and computational efficiency, particularly crucial for resource-constrained deployment scenarios.

Recent advances in structural design have enabled the development of compact AMC networks through module recombination and NAS. Representative studies demonstrate 80%-90% parameter reduction while maintaining baseline accuracy by integrating specialized components (e.g., parameter estimation modules, grouped convolutions) or NAS-driven optimization [10], [16]–[18]. Nevertheless, critical limitations persist: manual architectural engineering necessitates domain-specific expertise, NAS-based methods require intensive computational resources, and excessive compression frequently degrades recognition accuracy. To address these challenges, researchers are increasingly combining quantization techniques with knowledge distillation frameworks, enabling precision-preserving efficiency optimization through bit-width reduction and cross-model knowledge transfer.

B. Methods Based on Model Compression and Knowledge Transfer

Lightweight automatic modulation classification (AMC) methods primarily rely on pruning, quantization, and knowledge distillation. In pruning, Tu *et al.* [19] proposed an activation-guided pruning strategy to significantly compress

the VT-CNN2 model while maintaining classification accuracy. Zhang *et al.* [18] achieved parameter reduction in the PET-CGDNN model through sparse pruning without performance degradation. For quantization, researchers such as Tridgell *et al.* [20] implemented ternary weight quantization ($\{-1, 0, +1\}$) for real-time inference on radio-frequency system-on-chip platforms, though full-precision models retained accuracy advantages. KD frameworks often involve transferring insights from complex architectures to lightweight counterparts, balancing computational efficiency and performance. Challenges persist in maintaining robustness under dynamic channel conditions and designing efficient distillation topologies [18]–[20]. However, quantization relies on hardware-specific calibration, pruning compromises structural integrity, and knowledge distillation is constrained by teacher-student architectural alignment.

C. Weakly Supervised Learning-Based AMC

Weakly-supervised learning aims to train models with limited annotation information, including semi-supervised learning and self-supervised learning methods. In the area of AMC under semi-supervised learning, Li *et al.* [21] adopted a GAN-based method. A generator was used to generate fake samples, and a discriminator was used to judge the authenticity and modulation type of the samples. Dong *et al.* [22] proposed the SSRCNN, which introduced the Kullback-Leibler (KL) divergence loss and cross-entropy loss for the unlabeled samples. However, when the number of labeled samples is small, it is difficult to provide reliable pseudo-labels for the unlabeled samples. Liu *et al.* [23] used self-supervised contrastive learning (CL) to pre-train the unlabeled samples, constructing positive pairs through rotation augmentation. However, these methods face challenges including error accumulation in pseudo-labels, modulation distortion from augmentation-induced time-frequency feature disruptions, high computational costs in contrastive frameworks, and static encoders' limited adaptability to dynamic environments.

As mentioned above, existing AMC methods face efficiency-accuracy tradeoffs akin to quantization/pruning/KD limitations, compounded by error accumulation in weakly supervised paradigms. Our ALWNN network and its few-shot variant MALWNN resolve these conflicts, delivering SOTA accuracy with ultra-low computation while excelling in generalization and operational efficiency [24]–[26].

III. SIGNAL MODEL AND PROBLEM FORMULATION

The modulation procedure relocates the spectrum of the baseband signal to a carrier signal of higher frequency. This facilitates the encoding and transmission of the baseband signal's information without disturbances. Moreover, it allows the signal to be adapted to the channel environment. A comprehensive depiction of the received signal can be articulated in this way:

$$r(t) = x(t) * c(t) + n(t), \quad (1)$$

In the given formula, $x(t)$ stands for the transmitted signal in the absence of noise, $c(t)$ symbolizes the channel impulse response, and $n(t)$ is indicative of the noise, like Additive White Gaussian Noise (AWGN). The received signal $r(t)$ can be divided into its real and imaginary components, where the real component signifies the In-phase (I) channel and the imaginary component corresponds to the Quadrature (Q) channel. The issue of Deep Learning-based AMC can be described as:

$$\hat{y} = \arg \max_{y \in \mathbf{Y}} f(y|\mathbf{r}; \theta), \quad (2)$$

In this scenario, y denotes the actual modulation type, and \hat{y} stands for the predicted modulation type; \mathbf{Y} is the pool of modulation types; $f(\theta)$ is the transformation function that maps samples to modulation types, where θ symbolizes the model weight. In the sphere of Deep Learning and Automatic Modulation Classification, the main objective is to design a DL model, represented by θ , that strikes an optimal balance between high precision and low complexity.

IV. ALWNN AND MALWNN

In this section, the Adaptive Lightweight Wavelet Neural Network (ALWNN) is first introduced, and then the MALWNN framework is presented.

A. Lightweight Adaptive Wavelet Neural Network

The architecture of the ALWNN model is depicted in Figure 1. In the input phase, the raw data from the signal samples is converted into a tensor matrix of dimensions $N * 1 * 2 * L$, where N is indicative of the batch size and L represents the data length. The model first integrates I/Q channel data through depthwise separable convolutions, then extracts features via multi-level convolutional layers. An adaptive wavelet network performs multi-scale decomposition: iteratively refining low-frequency components while analyzing high-frequency components through global average pooling. Finally, hierarchical features are concatenated into a vector and processed by fully connected layers for classification.

1) *Initial Convolutions*: The signal employing I/Q modulation consists of two components, In-phase (I) and Quadrature (Q), which are orthogonal to each other. To encapsulate the interplay between the I channel and the Q channel, it's crucial to transform the tensor dimension signal from $(2, L)$ to a tensor of dimension $(1, L)$. This transformation was accomplished through the application of a deep convolutional layer and a pointwise convolutional layer. Within this deep convolutional layer, we utilized a total of 64 filters to amplify the variation of the features being extracted. In an effort to derive more advanced features, we applied an additional deep convolutional layer and a pointwise convolutional layer. As a result of this processing, the tensor's shape evolved from the initial state of $(N, 1, 2, L)$ to a more complex form of $(N, 64, L)$.

2) *Adaptive Wavelet*: The wavelet transform is a method that decomposes signals into components of different frequencies, enabling precise analysis at various scales by tweaking scale and shift parameters. It is particularly effective for

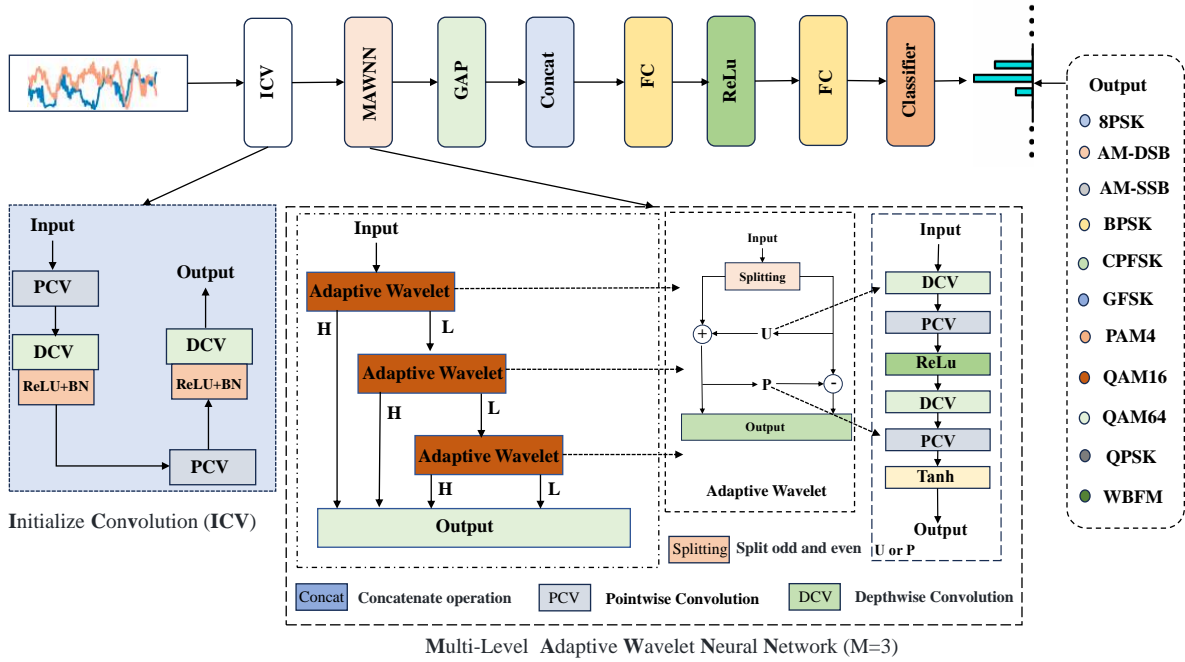


Fig. 1: Architecture of our proposed ALWNN.

transient signal analysis, offering insights into signal characteristics at multiple resolutions. Adaptive wavelets, an evolution of traditional wavelets, maintain core properties while introducing a flexible, dynamic approach to signal analysis. They adapt to the unique features of a signal, processing input r to produce approximation c and detail d coefficients through a structured three-phase approach.

Splitting: The input signal r is segmented into two distinct sections, with one comprising even-indexed components r_e and the other odd-indexed components r_o . This division is achieved through a Split function, which categorizes the data into these even and odd segments based on their indices. It can be expressed as:

$$\begin{aligned} [r_o, r_e] &= \text{Split}(r) \\ r_o[k] &= r[2k + 1] \\ r_e[k] &= r[2k] \end{aligned} \quad (3)$$

Predictor: Leveraging the time-frequency relationship inherent in the signal, the Predictor $P(\cdot)$ is employed to estimate r_o using r_e . The inherent correlation between r_o and r_e means that a well-chosen predictor $P(\cdot)$ can accurately forecast r_o , capturing the high-frequency details through the discrepancy between the actual and predicted values. This procedure can be articulated as:

$$d = r_o - P(r_e) \quad (4)$$

where d signifies high-frequency features, indicating the difference between r_o and $P(r_e)$.

Updater: The Updater employs $U(\cdot)$ to refine r_e , integrating the high-frequency details d into $U(\cdot)$ for enhancing the even components. This process of updating r_e enables it to more

accurately represent the low-frequency aspects of the original signal r . This mechanism can be illustrated as follows:

$$c = r_e + U(d) \quad (5)$$

In classical wavelet transformations, functions $P(\cdot)$ and $U(\cdot)$ assume basic linear shapes. As an example, the elementary Haar wavelet is articulated as:

$$\begin{aligned} d &= r_o - r_e \\ c &= r_e + \frac{1}{2}d \end{aligned} \quad (6)$$

Nevertheless, conventional wavelet transformation techniques are not adaptable and don't fully utilize the benefits of data-driven deep learning. The static $P(\cdot)$ and $U(\cdot)$ functions could be substituted with neural networks for improved flexibility. This approach allows for the adaptive determination of wavelet coefficients, thereby overcoming the limitation of traditional wavelet bases which cannot be optimized through backpropagation.

3) *Multi-Level Adaptive Wavelet Neural Network:* Initial convolutional extraction ensures each channel in the feature map \mathcal{F} encapsulates diverse feature information. Direct pooling of these feature vectors risks significant data loss. To mitigate this, adaptive wavelet transformation is applied using learnable $P(\cdot)$ and $U(\cdot)$. Consequently, \mathcal{F} is decomposed into its low-frequency and high-frequency components, expressed as:

$$\begin{aligned} [L_o^{(j)}, L_e^{(j)}] &= \text{Split}(L^{(j)}) \\ H^{(j+1)} &= L_o^{(j)} - P(L_e^{(j)}) \\ L^{(j+1)} &= L_e^{(j)} + U(H^{(j+1)}) \end{aligned} \quad (7)$$

In this context, j indicates the iteration of adaptive wavelet transformations, with H and L representing high-frequency and low-frequency components, respectively. Notably, $L^{(0)}$ refers to the initial feature map derived from the first convolutional layer.

Figure 1 illustrates the architecture of $P(\cdot)$ and $U(\cdot)$. The process starts with reflection padding of the input low-frequency component to preserve sequence length post-convolution. This is followed by integration of feature map information via a depthwise convolution and a pointwise convolution layer, with ReLU activation function facilitating the polynomial fitting across different channels.

After conducting M levels of wavelet transformation, we obtain M high-frequency components ($H^{(1)}, H^{(2)}, \dots, H^{(M)}$) and M low-frequency components ($L^{(1)}, L^{(2)}, \dots, L^{(M)}$). Global average pooling is applied to these components, transforming them from $\mathbb{R}^{C \times L}$ to feature vectors $\mathcal{F}_{GAP} \in \mathbb{R}^{C \times 1}$. Concatenating these vectors yields the final feature vector X , with T denoting the vector length, as shown in:

$$\mathcal{F}_{GAP}(j) = \frac{1}{T} \sum_{i=0}^{T-1} \mathcal{F}_{i,j}, \quad (8)$$

$$X = \text{Concat}\left(L_{GAP}^{(M)}, H_{GAP}^{(1)}, \dots, H_{GAP}^{(M)}\right).$$

4) *Loss Function*: The traditional wavelet scheme, constrained by predetermined formulas for predictors and updaters, couldn't optimally harness data. Alternatively, neural networks, renowned for their advanced learning abilities, improve this framework. The adaptive wavelet model is streamlined into two primary components: the detail loss function and the approximation loss function.

$$\text{Loss}_L = \sqrt{\sum_i (r_o[i] - P(r_e)[i])^2} \quad (9)$$

$$\text{Loss}_H = \sqrt{\sum_i (r_o[i] - r_e[i] - U(r_e)[i])^2} \quad (10)$$

The ALWNN training loss function integrates cross-entropy with Loss_L for approximation and Loss_H for detail reduction, optimizing data representation.

$$L(\theta) = \lambda_1 \sum_{i=0}^{M-1} |H^{(i)}| + \lambda_2 \sum_{i=0}^{M-2} \|L^{(i)} - L^{(i+1)}\|_2 - \log p_\theta(y = n|x) \quad (11)$$

The batch training strategy is encapsulated in pseudocode detailed within Algorithm 1, where λ_1 and λ_2 serve to adjust the strength of regularization. K specifies the variety of signal modulation categories, and M indicates the depth of decomposition.

B. Few-Shot AMC Framework

Figure 2 presents the framework structure of MALWNN. Our system is comprised of a few-shot training module and a few-shot testing module. The training module contains a data processing section, a feature extraction portion, and a

Algorithm 1 ALWNN Batch Training

Require: Training data \mathbf{r} with targets \mathbf{y} , model weights \mathbf{w} , decomposition levels M , and regularization terms λ_1, λ_2 .

- 1: The initial convolutional layer processes the data, resulting in feature maps, denoted as \mathbf{F} .
 - 2: **for** each $k \in [1, M]$ **do**
 - 3: Split(\mathbf{F}) partitions \mathbf{F} into \mathbf{F}_{even} and \mathbf{F}_{odd} .
 - 4: Compute prediction: $\mathbf{H}_k = \mathbf{F}_{\text{odd}} - P_k(\mathbf{F}_{\text{even}})$
 - 5: Update: $\mathbf{L}_k = \mathbf{F}_{\text{even}} + U_k(\mathbf{H}_k)$
 - 6: Calculate regularization terms: $\mathcal{L}_H = \mathcal{L}_H + \lambda_1 \cdot \text{mean}(|\mathbf{H}_k|)$; $\mathcal{L}_L = \mathcal{L}_L + \lambda_2 \cdot |\text{mean}(\mathbf{L}_k) - \text{mean}(\mathbf{F})|$
 - 7: Concatenate feature vector: $\mathbf{f} = [\mathbf{f}; \text{GAP}(\mathbf{H}_k)]$
 - 8: Update \mathbf{F} to \mathbf{L}_k : $\mathbf{F} = \mathbf{L}_k$
 - 9: **end for**
 - 10: Perform feature fusion: $\mathbf{f} = [\mathbf{f}; \text{GAP}(\mathbf{F})]$.
 - 11: calculate $\mathcal{L}_{CE} : -\sum_{j=1}^K y_j \log(\hat{y}_j)$
 - 12: The final loss is $\mathcal{L} = \mathcal{L}_{CE} + \mathcal{L}_H + \mathcal{L}_L$. Compute the gradients $\frac{\partial \mathcal{L}}{\partial \theta}$ during back-propagation and update the model parameters: $\theta = \theta - \eta \frac{\partial \mathcal{L}}{\partial \theta}$.
-

class prototype component. The data processing part primarily extends or truncates the signals to guarantee a signal length of 1024. The feature extraction module herein is the ALWNN referred to previously, which is capable of fully extracting the features of various dimensions of the signal while reducing the parameter count and computational complexity of the feature extraction network. The signal samples are mapped into a unified feature measurement space via the feature extraction module, and the class prototype module conducts distance measurement and ascertains the modulation pattern of the signal to be identified. The Euclidean distance is employed as the distance measurement approach in this paper. Owing to the attainment of meta-knowledge, this method can sustain favorable performance even with an insufficient number of samples. The fundamental structure of the testing module resembles that of the training module, with the exception that no backpropagation of gradients is performed. Notably, the testing module directly yields the classification outcome, whereas the training result outputs the loss function value.

1) *Meta Training*: The training module conducts the training of the parameter θ of ALWNN. In this stage, the training is carried out episodically. Each episode, marked as ϵ , consists of a support set for prototype generation and a query set for modulation prediction and parameter update. To generate the support set and query set for each episode, we first randomly select n categories from the source dataset. Then, within each selected category, we further randomly pick k instances. Here, n represents the total number of classes within the support set, commonly referred to as n -way, and k represents the number of data samples for each class (way), known as k -shot. The total number of episodes, denoted as N_ϵ , can be determined by the following formula:

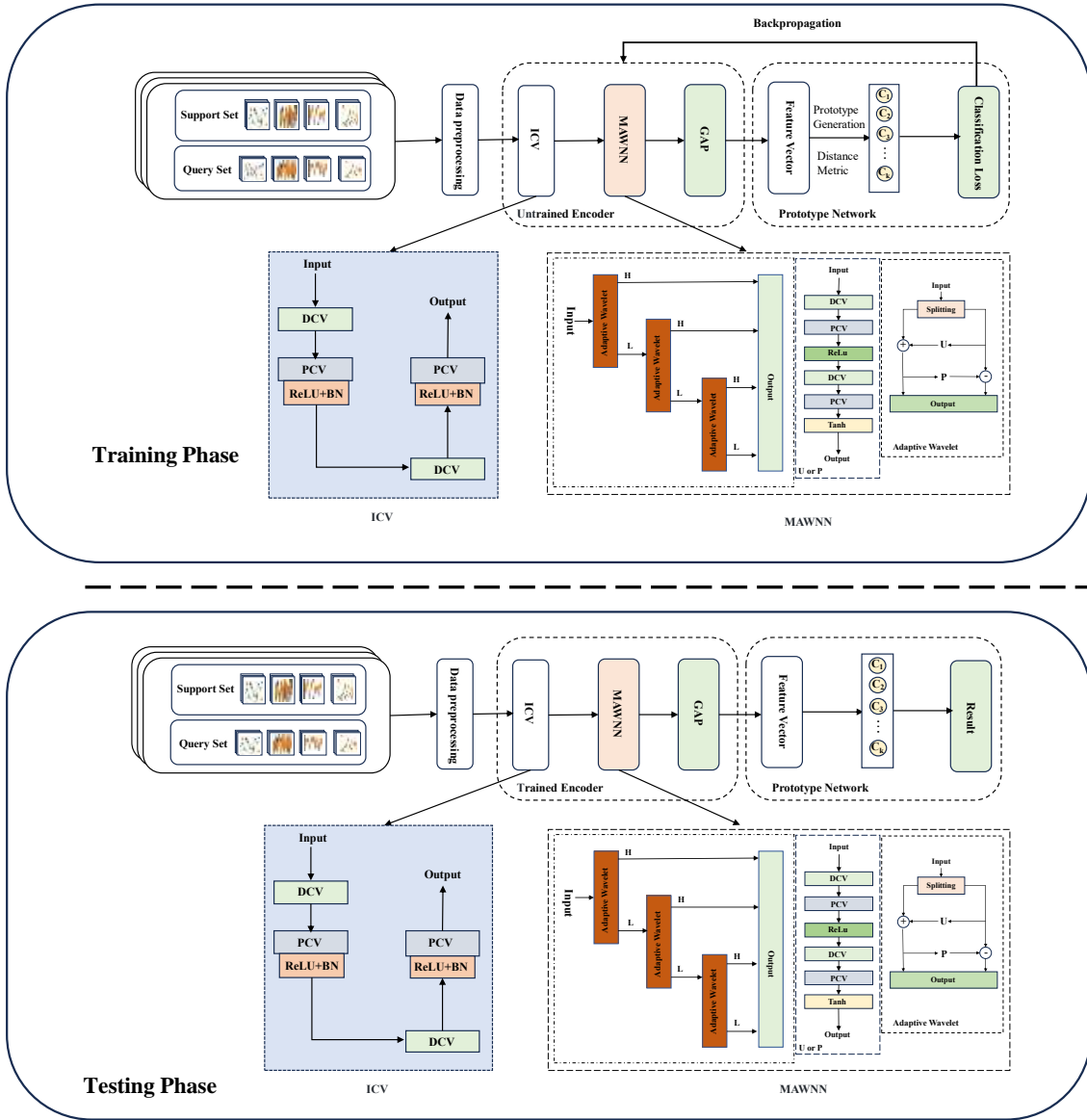


Fig. 2: Architecture of our proposed few shot framework MALWNN.

$$N_{\epsilon} = \frac{p_{train} \cdot N}{N_S + N_Q} \cdot N_{epoch} \quad (12)$$

Among them, N represents the total quantity of data. p_{train} refers to the proportion of the training dataset. N_S stands for the number of support sets, and N_Q represents the number of query sets. N_{epoch} denotes the number of training epochs, The N annotated data used as input, denoted as $D = \{(x_1, y_1), \dots, (x_N, y_N)\}$. In each episode, the pre-processing module guarantees a fixed signal length by means of signal truncation and expansion. Thereafter, the data of the support set and the query set are divided into small segments as previously depicted and then input into the encoder of the ALWNN network. For the support set, the prototype p_l is generated by averaging the feature vectors extracted from the annotated dataset S_l that belongs to class l , as shown in the

following equation.

$$p_l = \frac{1}{|D_l|} \sum_{(x_j, y_j) \in D_l} f_{\theta}(x_j) \quad (13)$$

The feature vectors extracted from the query set are classified using the generated prototypes based on a distance function d , which can be methods such as the Euclidean distance or cosine similarity. In this paper, the Euclidean distance function is used as the distance function. Based on the softmax function of the distance between the query point x and the prototypes in the embedding space, we generate a distribution over classes. The formula for this distribution is as follows:

$$p_{\theta}(y = l|x) = \frac{\exp(-d(f_{\theta}(x), p_l))}{\sum_{l'} \exp(-d(f_{\theta}(x), p_{l'}))} \quad (14)$$

Within each training episode, the parameter θ is iteratively updated using the Adam optimizer to minimize the loss function. The specific training algorithm can be found in Algorithm 2. The function is expressed as:

$$L(\theta) = -\log p_{\theta}(y = l|x) + \lambda_1 \sum_{i=0}^{M-1} |H^{(i)}| + \lambda_2 \sum_{i=0}^{M-2} \left\| L^{(i)} - L^{(i+1)} \right\|_2 \quad (15)$$

Algorithm 2 Meta Training Workflow

1: n Is the Number of Classes per Episode, E Is the Selected n Classes for Episode, N_S Is the Number of Support samples per Class, N_Q Is the Number of Query samples per Class, \hat{m} Is the Bias-Corrected Moving Average of the Gradients, \hat{v} Is the Bias-Corrected Moving Average of the Squared Gradients, α Is the Learning Rate and ϵ Is a Small Value Used for Numerical Stability. Random uniform(D, N) Denotes Uniform and Random Selection of N Values From the D Set. Signal Length(D, z) Denotes the Adjustment of All x Lengths in Set D to z .

2: **Input:** Training set $D_{train} = \{(x_1, y_1), \dots, (x_N, y_N)\}$
3: **Output:** Trained ALWNN f_{θ}
4: **for** $l = 1, \dots, n$ **do**
5: $D_{support} \leftarrow$ Random uniform(D_{E_l}, N_S)
6: $D_{query} \leftarrow$ Random uniform($D_{E_l} \setminus D_{support}, N_Q$)
7: $D_{support} \leftarrow$ Signal Length($D_{support}, z_m$)
8: $D_{query} \leftarrow$ Signal Length(D_{query}, z_m)
9: $p_l \leftarrow \frac{1}{|D_l|} \sum_{(x_j, y_j) \in D_l} f_{\theta}(x_j)$
10: **end for**
11: $L \leftarrow 0$ Initialize loss L
12: **for** $l = 1, \dots, n$ **do**
13: **for** $(x, y) \in D_{query}$ **do**
14: $\theta \leftarrow \theta - \frac{\alpha}{\sqrt{\hat{v} + \epsilon}} \hat{m}$
15: **end for**
16: **end for**

2) *Meta Testing:* The testing module utilizes the model weights trained through training truncation, which remain fixed during the testing process. In the meta-testing stage, both the support set and the query set contain unseen modulation methods, enabling us to evaluate the model’s adaptability to new domains and its generalization ability. The signal length processed by the data processing module is 1024, which is the signal length of RadioML2018.01a. In most few-shot learning (FSL)-based methods, the commonly adopted configuration for the support set is the 5-shot setting, meaning that the support set contains five data samples. The testing module uses the trained ALWNN model to generate n' prototypes, where n' represents the number of target classes for testing. The query set used for inference is classified based on the Euclidean distance between the embedding vectors and the prototypes.

V. NUMERICAL RESULTS

A. Datasets

The experiment was carried out using the RML2016.10a, RML2016.10b, and RML2018.01a datasets, which were synthesized via GNU Radio to accurately mimic the wireless conditions in the real world, incorporating elements like multipath fading, sampling rate offset, additive white noise, and the central frequency offset of the wireless channel. The RML2016.10a dataset contains 11 prevalent modulation types, totaling 220,000 modulated signals, including 8PSK, QPSK, BPSK, QAM64, QAM16, CPFSK, GFSK, 4PAM, WBFM, AM - SSB, and AM - DSB. The RML2016.10b dataset, on the other hand, holds 12 million signals across 10 types, excluding AM - SSB, and in both these datasets, the SNR ranges from -20dB to 18dB in 2dB steps, with each signal stored as a 2×128 matrix representing the in-phase and quadrature parts of the modulated signal samples. The RML2018.01a dataset is larger and more complex, featuring 24 modulation formats and 255,590,400 modulated signals, with an SNR from -20dB to 30dB at 2dB intervals and a signal size of 2×1024 . It simulates more channel impairments, increasing classification difficulty, and also incorporates more high-order and analog modulation formats, making classification highly challenging.

B. Experimental Settings

In the experiment of lightweight ALWNN, the datasets were partitioned, with 60% being allocated for training, 20% for validation, and the remaining 20% serving as the test set. These partitions were employed to train and evaluate all tasks. Stratified sampling was carried out for different signal-to-noise ratios of various modulation formats. Each signal-to-noise ratio of different format signals was also divided in a ratio of 6:2:2. This experiment was implemented based on the Pytorch 2.0 framework. In the experiments concerning RML2016.10a and RML2016.10b, we utilized an Adam optimizer with a batch size of 256 to train the proposed network. The initial learning rate was set at 0.001 for this experiment. The regularization term coefficients λ_1 and λ_2 were equal to 0.01. If the loss of the validation set failed to decrease within a span of five epochs, an early termination of the training process would be triggered. For the RML2016.10A and RML2016.10b datasets, the number of layers of the adaptive wavelet transform was set to 1. In contrast, for the RML2018.01a dataset, the number of layers of the adaptive wavelet transform was set to 3. This is because when the signal length of the data is 128, a single layer of the adaptive wavelet transform is sufficient to extract features, while a signal length of 1024 renders a single layer far from adequate. The sizes of the depth convolutional kernels for initializing the convolutional layers were 2×7 and 1×5 respectively. The depth convolutional kernels for the $U(\cdot)$ and $P(\cdot)$ parts were of size 1×5 . The kernels for pointwise convolutions throughout the model were of size 1×1 . All experiments were conducted using NVIDIA CUDA with a GeForce RTX 4090 GPU.

In the experiment of MALWNN, we selected the RML2018.10a dataset and divided it proportionally. Among

it, 70% of the data was used for training the model, 10% of the data served as the validation set for optimizing the model parameters, and the remaining 20% of the data was used as the test set to evaluate the model performance. This experiment was implemented based on the Pytorch 2.0 framework. During the training process, we used an Adam optimizer with a batch size set to 512 to train and optimize the proposed network. Meanwhile, the initial learning rate of the experiment was set to 0.001, and the regularization term coefficients λ_1 and λ_2 were both set to 0.001. In view of the characteristics of the dataset, the number of layers of the adaptive wavelet transform was determined to be 3, and the Euclidean distance metric was adopted as the distance measurement method. The other relevant settings remained the same as those mentioned above.

C. Classification Performance of ALWNN

We compared our ALWNN model with six benchmark models using the RadioML2016.10a and RadioML2016.10b datasets. The primary benchmark models include CLDNN [7], MCLDNN [8], ICAMC [27], MCNET [28], AMC-Net [29], CDSCNN [30]. All methods employed the original I/Q samples as input.

As shown in Table I, we utilized multiple key metrics to conduct a detailed and comprehensive evaluation and comparison analysis of our self-developed Adaptive Wavelet Neural Network (ALWNN) model against other benchmark models on the RadioML2016.10a and RadioML2016.10b datasets. The selected metrics cover important dimensions such as accuracy, kappa coefficient, Macro - F1 score (MF1), number of parameters, floating - point operations per second (FLOPS), and normalized multiply - accumulate complexity (NMACC).

Among them, the accuracy precisely reflects the average recognition accuracy level of the model under all SNR conditions and is one of the crucial fundamental metrics for evaluating the performance of the model. The kappa coefficient, as a statistical measure specifically used to evaluate the degree of classification consistency, in this context, its core function lies in accurately assessing the degree of fit and consistency between the model's classification results and the actual true annotation results. The Macro - F1 score (MF1) approaches from the perspective of comprehensive evaluation across multiple categories. By averaging the F1 values of each category, it enables us to comprehensively and evenly grasp the overall performance status of the model across multiple categories, effectively avoiding the problem of overlooking the overall performance balance due to excessive focus on some categories, thus providing a more comprehensive, objective, and accurate perspective for the comprehensive performance evaluation of the model. The number of parameters, to a certain extent, directly reflects the complexity of the model's structure and its information - carrying capacity, indirectly reflecting the scale and capacity characteristics of the model. The floating - point operations per second (FLOPS) emphasizes characterizing the level of computational efficiency of the model during operation, directly related to the actual demand for computational resources and the speed of resource con-

sumption when the model is running. The normalized multiply - accumulate complexity (NMACC) further clearly reflects the complex characteristics and resource demand tendencies of the model from a specific computational complexity dimension.

Especially noteworthy is that the accuracy performance of our developed Adaptive Wavelet Neural Network model is only slightly inferior to that of the optimal AMCNet model, demonstrating strong competitiveness. At the same time, compared with the baseline methods, the ALWNN model has achieved remarkable results in terms of computational efficiency and resource demand optimization. Specifically, its floating - point operations per second have been significantly reduced by 1.25 to 1.91 orders of magnitude, and the normalized multiply - accumulate complexity has also been significantly reduced by 0.81 to 1.6 orders of magnitude. This dual reduction in computational volume and complexity is expected to sharply reduce the inference latency of the model on low - computational - power central processing units (such as Raspberry Pi or microcontrollers) from the original several seconds to the millisecond level. At the same time, it can also effectively alleviate the storage pressure and computational resource demand burden on terminal devices. These series of advantages make the practical application of the adaptive modulation and coding method in wireless communication systems possible, laying a solid foundation for its wide promotion and application, and is expected to promote the further development and innovation in the field of wireless communication technology. Figure 3, Figure 4 and Figure 5 clearly present the comparison of the classification performance between our self-developed Adaptive Wavelet Neural Network (ALWNN) model and other benchmark models under different SNR situations on the RadioML2016.10a, RadioML2016.10b and RadioML2018.01a datasets. It can be clearly seen from the presented data that under numerous different SNR conditions, our ALWNN model demonstrates outstanding performance advantages and its performance surpasses that of most of the models it is compared with, which fully proves the high efficiency and reliability of this model in complex signal classification tasks.

D. Ablation Study

The results of the ablation experiment are presented in Table II and Table III. In Table II, a study was carried out on the impact of each module of ALWNN on the model performance. It can be clearly observed from Table II that the AWN module has an extremely significant impact on the model performance. This is due to its ability to extract features from multiple dimensions, thus enhancing the model's understanding and processing ability of the data. Next is the initialization convolution module, which also plays a crucial role in improving the model performance. Furthermore, the introduction of the attention mechanism and the increase in the number of AWN stages can also improve the model performance, but this will correspondingly lead to an increase in the number of parameters. The experiment in Table III shows that for the RML2018.01a dataset, the model can

TABLE I: Combined Performance of All Methods on Different Datasets

Dataset	Model	Accuracy	MF1	Kappa	Parameters(K)	MACC(M)	FLOPS(M)	Inference time (ms/sample)
RML2016.10a	ALWNN	0.6214	0.6423	0.5815	9.899K	0.53M	0.52M	0.045
	CLDNN	0.5871	0.6091	0.5447	160K	5.74M	11.986M	0.225
	MCLDNN	0.6203	0.6381	0.5803	380K	20.94M	41.876M	0.283
	ICAMC	0.5681	0.5983	0.5401	1210K	7.7M	15.403M	0.102
	AMC - Net	0.6251	0.6483	0.5885	470K	9.4M	18.799M	0.122
	CDSCNN	0.5920	0.6060	0.5512	860K	13M	25.998M	0.324
	MCNET	0.5600	0.5912	0.5382	120K	3.44M	9.289M	0.088
RML2016.10b	ALWNN	0.6393	0.6386	0.5992	9.7K	0.53M	0.52M	0.047
	CLDNN	0.6021	0.6088	0.5972	160K	5.74M	11.986M	0.216
	MCLDNN	0.6358	0.6412	0.6028	380K	20.94M	41.876M	0.282
	ICAMC	0.6243	0.6332	0.6023	1210K	7.7M	15.403M	0.106
	AMC - Net	0.6463	0.6487	0.6081	470K	9.4M	18.799M	0.132
	CDSCNN	0.6288	0.626	0.587	860K	13M	25.998M	0.323
	MCNET	0.6074	0.6102	0.5883	120K	3.44M	9.289M	0.082
RML2018.01a	ALWNN	0.6259	0.6266	0.6097	31K	2.12M	2.132M	0.090
	CLDNN	0.5549	0.5602	0.5432	0.84M	30.135M	68.916M	1.431
	MCLDNN	0.6242	0.6222	0.6012	0.38M	210.94M	241.876M	1.963
	ICAMC	0.5839	0.5913	0.5723	8.21M	53.9M	93.85M	0.125
	AMC - Net	0.6263	0.6287	0.611	28.2M	56.4M	197.88M	1.231
	CDSCNN	0.6088	0.6166	0.57	56M	121.3M	205.8M	2.032
	MCNET	0.5619	0.5645	0.5422	120K	7.44M	11.9M	0.108

achieve the best performance when $M = 3$. When $M = 0$, the recognition accuracy is at the lowest level, and the model has difficulty in accurately classifying the data. After reaching the optimal state at $M = 3$, as the value of M further increases, the accuracy of the model generally remains stable and no obvious upward trend appears. At the same time, the number of parameters increases significantly. We infer that the reason for this phenomenon is that the signal length of RML2018.01a is 1024. When the number of decomposition layers is low, the model cannot efficiently extract multi-dimensional features. When the number of decomposition stages exceeds a certain threshold, the data features have been fully extracted, so it is difficult to further improve the classification performance.

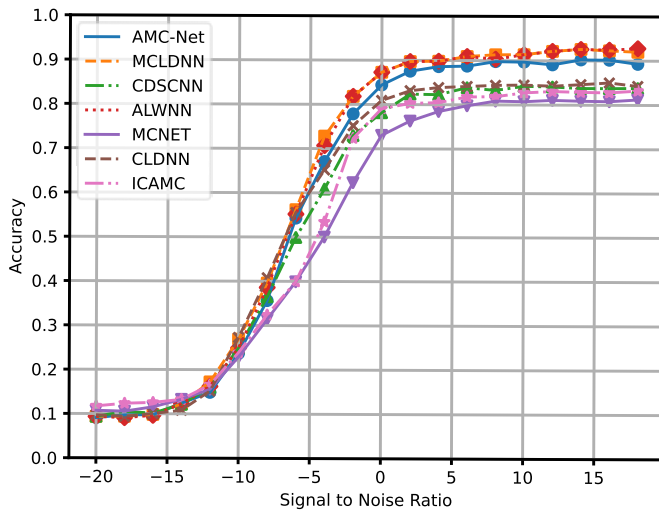


Fig. 3: Classification accuracy on different SNR of ALWNN and other models on RML2016.10a.

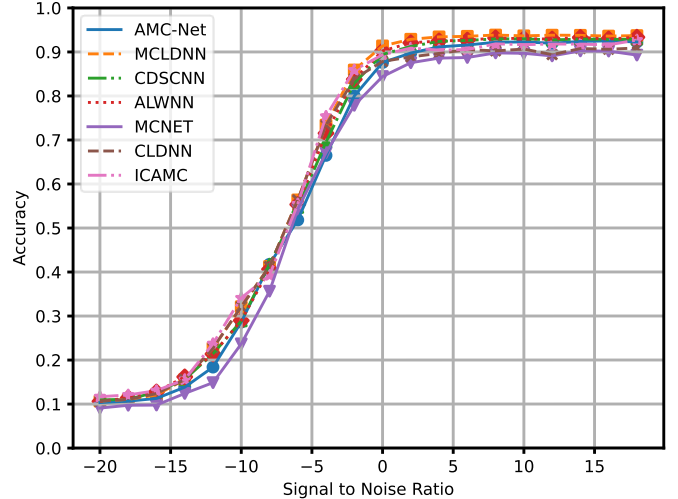


Fig. 4: Classification accuracy on different SNR of ALWNN and other models on RML2016.10b.

E. Few Shot Framework Evaluation

This experiment evaluates the adaptive performance of the proposed MALWNN framework to new modulation types. Leveraging the rapid transfer capability of meta-learning (e.g., when software-defined radios require dynamic recognition of new modulations), we established a test scenario: 10 modulation types were randomly selected from 24 candidates for model training, while 5 unseen types were sampled from the remaining 12 for testing (see Table IV). Adopting the 5-shot configuration aligned with few-shot learning benchmarks, each test group underwent 100 random trials with averaged precision calculation. The training and testing datasets contained approximately 1.3 million and 500,000 sample frames respectively.

Figure 6 depicts the precision results of three test cases,

TABLE II: THE ABLATION STUDIES

Method	Ablation part	Average accuracy	MF1	kappa	Number of Parameters(M)
ALWNN	-	62.59%	62.66%	60.97%	0.031
ALWNN - A	add attention	62.60% (0.015% ↑)	62.94% (0.44% ↑)	60.93% (0.14% ↓)	0.08 (110% ↑)
ALWNN - B	w/o CV	60.56% (3.240% ↓)	60.36% (3.67% ↓)	59.60% (2.24% ↓)	0.025 (0.6% ↓)
ALWNN - C	w/o AWN	54.16% (13.53% ↓)	54.45% (13.10% ↓)	53.12% (12.87% ↓)	0.015 (51.61% ↓)
ALWNN - D	ADD Harr	58.39% (6.71% ↓)	59.13% (5.63% ↓)	57.23% (6.13% ↓)	0.029 (6.45% ↓)
ALWNN - E	add FFT	60.99% (2.55% ↓)	60.73% (3.08% ↓)	58.59% (3.90% ↓)	0.032 (3.22% ↑)
ALWNN - F	M=1	60.50% (3.33% ↓)	60.30% (3.76% ↓)	58.89% (3.41% ↓)	0.02336 (24.64% ↓)

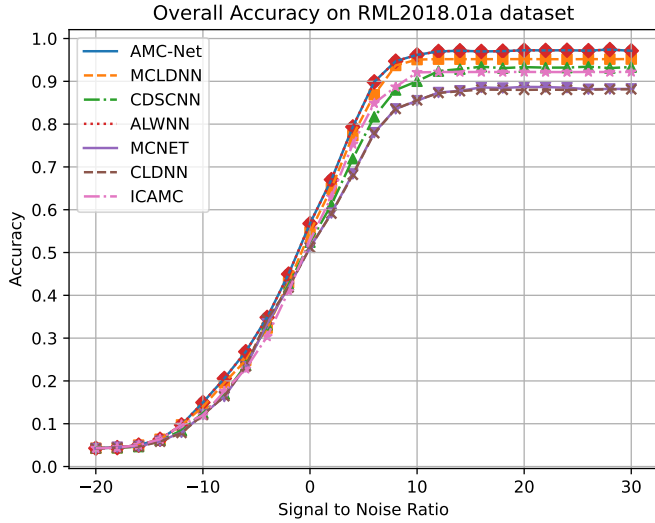


Fig. 5: Classification accuracy on different SNR of ALWNN and other models on RML2018.01a.

TABLE III: Sensitivity Analysis of Parameter M

Num of Level	Average accuracy	MF1	Number of Parameters(K)
$M = 0$	54.16%	54.45%	15.19
$M = 1$	58.50%	59.30%	23.36
$M = 2$	61.59%	61.82%	35.39
$M = 3$	62.59%	62.66%	57.08
$M = 4$	62.60%	62.66%	81.54
$M = 5$	62.61%	62.63%	129.42

illustrating that in the testing phase, the average precision of the five modulation methods in the high signal-to-noise ratio region was approximately 84%. The variation in accuracy among different test cases was affected by the modulation methods used in the training phase. When similar modulation methods appeared in the training phase, the model performance often tended to be better in the testing phase, such as case D and case E. In case B, all the modulation methods in the training phase were digital modulations, while all those in the testing phase were analog modulations, so the testing performance was relatively poor.

Figure 7 presents the experimental results of investigating the impact of the Shot value on the model performance in the testing phase. For the five-class classification problem in the testing phase, the Shot values were 1, 5, 10, 15, and 20 respectively. The results showed that the accuracy increased with the increase of the Shot value. When the Shot value was greater than or equal to 15, our method achieved an accuracy rate of 95%, demonstrating that the proposed framework can

achieve good performance even with only a small number of datasets.

In this section, to verify the performance superiority of the algorithm proposed in this paper compared with other few-shot modulation recognition algorithms, we selected few-shot modulation recognition algorithms based on data augmentation (DA) and transfer learning (TL) for comparison experiments. Additionally, three other meta-learning algorithms were chosen, namely the relation network (RN), matching networks (MN), and model-agnostic meta learning (MAML).

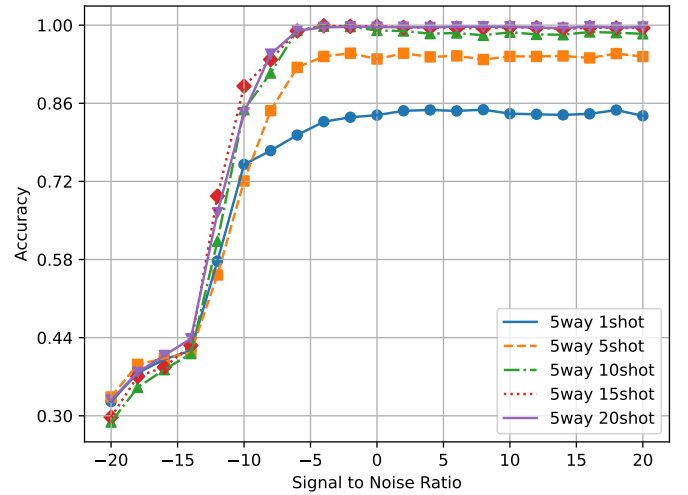


Fig. 6: Classification accuracy on different shot of on Case A.

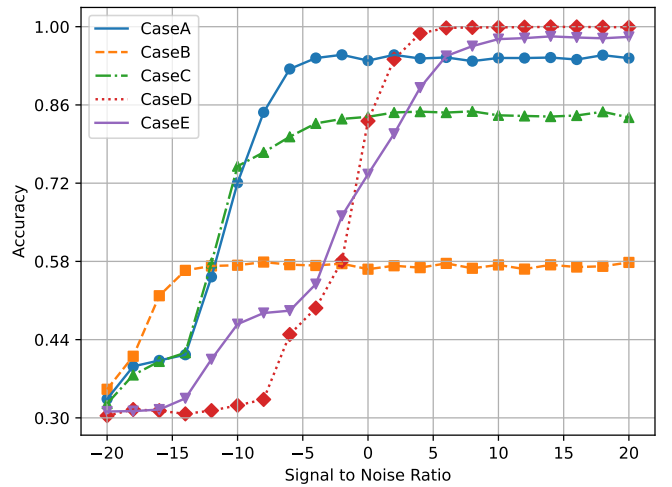


Fig. 7: Classification accuracy on different SNR on different case.

TABLE IV: Experimental data set diversity

case	Train set	Test set
A	4ASK, 8ASK, QPSK, 8PSK, 32PSK, 32APSK, 128APSK, 32QAM, 64QAM, 256QAM	OOK, BPSK, 16APSK, 16QAM, GMSK
B	OOK, 4ASK, BPSK, 8PSK, 16PSK, 32PSK, 64APSK, 64QAM, 16QAM, 128APSK	AM - DSB - SC, AM - SSB - WC, AM - DSB - WC, FM, AM - SSB - SC
C	OOK, 4ASK, BPSK, 16PSK, 8PSK, 16APSK, 32APSK, 128QAM, 64QAM, 32QAM	16QAM, QPSK, 8PSK, 16PSK, 32PSK
D	OOK, 8ASK, 16PSK, 16APSK, 32APSK, AM - SSB - SC, AM - DSB - WC, 128APSK, 32QAM, GMSK	4ASK, 8PSK, FM, 256QAM, 32APSK
E	ALL	ALL

TABLE V: INFERENCE TIME PER SAMPLE ON EDGE DEVICE

Methods	Inference time per sample on edge device (unit: s)			
	Batchsize 2	16	128	1024
ALWNN (proposed)	6.85×10^{-3}	1.43×10^{-3}	9.84×10^{-4}	8.1×10^{-4}
MCLDNN	6.78×10^{-2}	1.74×10^{-2}	9.99×10^{-3}	7.97×10^{-3}
CLDNN	6.32×10^{-2}	1.69×10^{-2}	8.45×10^{-3}	6.88×10^{-3}
MCNet	4.74×10^{-3}	1.2×10^{-3}	10.25×10^{-4}	8.40×10^{-4}
ICAMC	6.46×10^{-2}	1.55×10^{-2}	8.02×10^{-3}	6.12×10^{-3}
AMCNet	7.23×10^{-2}	2.15×10^{-2}	7.22×10^{-3}	6.56×10^{-3}
CDSCNN	9.71×10^{-2}	4.21×10^{-2}	9.24×10^{-3}	8.42×10^{-3}

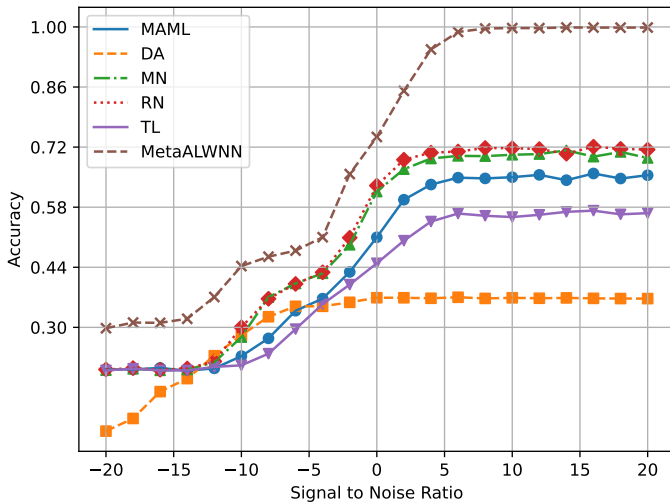


Fig. 8: Classification accuracy on different SNR of MALWNN and other models on CaseA.

The training and test sets in CaseA were utilized to train and test the models. To ensure the reliability of the experimental results, this sample set was adopted as the data source for both the DA and TL algorithms, as well as for the algorithm proposed in this paper and the RN, MN, and MAML algorithms. When focusing on five types of modulation signals and with the sample quantity of each type precisely set at five, the variation trend of the test recognition accuracy of our algorithm and the comparison algorithms with the change of signal-to-noise ratio is vividly illustrated in Figure 8.

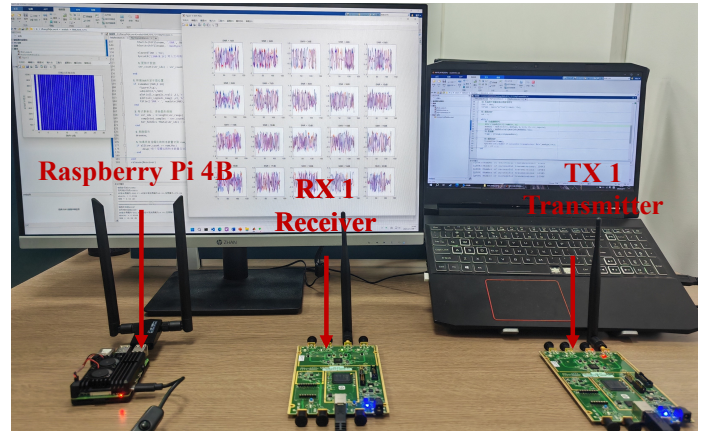


Fig. 9: AMC testbed via USRP 2901s and Raspberry Pi 4B.

VI. EXPERIMENTAL RESULTS

We conducted field experiments using USRP N2901 and Raspberry Pi 4B, evaluating the performance of our AMC method on the low-power Raspberry Pi. As shown in Figure 9, The experimental setup included two NI USRP 2901 transceivers (connected via USB 3.0 and Ethernet), a Raspberry Pi 4B, and an RTX 4090 GPU, capturing and processing real-world modulated signals such as 2ASK, FSK, AM, BPSK, QPSK, GMSK, 16QAM, and 64QAM. The test results are shown in Table V. Results showed that while ALWNN had low theoretical computational complexity, it was not the fastest model. Our proposed ULCNN exhibited limitations on the GPU but matched MCNet’s inference speed on edge devices, demonstrating better suitability for resource-constrained scenarios. Increasing batch sizes significantly reduced per-sample

inference latency due to parallelized processing and optimized resource utilization. ALWNN maintained robust accuracy and practical inference speed in real-world deployments.

VII. CONCLUSION

This paper proposes a lightweight AMC method ALWNN and a few-shot AMC framework MALWNN. Simulation results demonstrate that the proposed ALWNN achieves significant advantages in both accuracy and computational efficiency, while MALWNN also exhibits strong generalization capability and high precision, making them particularly suitable for edge computing scenarios with limited hardware resources and scarce training data. In future work, we will explore the implementation of AMC algorithms under multimodal data inputs.

ACKNOWLEDGEMENT

This work was supported by the National Key Research and Development Program of China (2020YFB2907500).

REFERENCES

- [1] B. Jdid, K. Hassan, I. Dayoub, W. H. Lim, and M. Mokayef, "Machine learning based automatic modulation recognition for wireless communications: A comprehensive survey," *IEEE Access*, vol. 9, pp. 57 851–57 873, 2021.
- [2] X. Wang, K. Tao, N. Cheng, Z. Yin, Z. Li, Y. Zhang, and X. Shen, "Radiodiff: An effective generative diffusion model for sampling-free dynamic radio map construction," *IEEE Transactions on Cognitive Communications and Networking*, pp. 1–1, 2024.
- [3] D. Zhu, V. J. Mathews, and D. H. Dettienne, "A likelihood-based algorithm for blind identification of qam and psk signals," *IEEE Transactions on Wireless Communications*, vol. 17, no. 5, pp. 3417–3430, 2018.
- [4] J. Ma and T. Qiu, "Automatic modulation classification using cyclic correlation spectrum in impulsive noise," *IEEE Wireless Communications Letters*, vol. 8, no. 2, pp. 440–443, 2019.
- [5] T. J. O'Shea, T. Roy, and T. C. Clancy, "Over-the-air deep learning based radio signal classification," *IEEE Journal of Selected Topics in Signal Processing*, vol. 12, no. 1, pp. 168–179, 2018.
- [6] F. Meng, P. Chen, L. Wu, and X. Wang, "Automatic modulation classification: A deep learning enabled approach," *IEEE Transactions on Vehicular Technology*, vol. 67, no. 11, pp. 10 760–10 772, 2018.
- [7] N. E. West and T. O'Shea, "Deep architectures for modulation recognition," in *2017 IEEE International Symposium on Dynamic Spectrum Access Networks (DySPAN)*, 2017, pp. 1–6.
- [8] J. Xu, C. Luo, G. Parr, and Y. Luo, "A spatiotemporal multi-channel learning framework for automatic modulation recognition," *IEEE Wireless Communications Letters*, vol. 9, no. 10, pp. 1629–1632, 2020.
- [9] L. Wang, X. Wu, Y. Zhang, X. Zhang, L. Xu, Z. Wu, and A. Fei, "Deepadain-net: Deep adaptive device-edge collaborative inference for augmented reality," *IEEE Journal of Selected Topics in Signal Processing*, vol. 17, no. 5, pp. 1052–1063, 2023.
- [10] L. Guo, Y. Wang, Y. Liu, Y. Lin, H. Zhao, and G. Gui, "Ultralight convolutional neural network for automatic modulation classification in internet of unmanned aerial vehicles," *IEEE Internet of Things Journal*, vol. 11, no. 11, pp. 20 831–20 839, 2024.
- [11] H. Lu, F. Lyu, J. Ren, H. Wu, C. Zhou, Z. Liu, Y. Zhang, and X. Shen, "Code⁺: Fast and accurate inference for compact distributed iot data collection," *IEEE Transactions on Parallel and Distributed Systems*, vol. 35, no. 11, pp. 2006–2022, 2024.
- [12] W. Kong, X. Jiao, Y. Xu, B. Zhang, and Q. Yang, "A transformer-based contrastive semi-supervised learning framework for automatic modulation recognition," *IEEE Transactions on Cognitive Communications and Networking*, vol. 9, no. 4, pp. 950–962, 2023.
- [13] L. Wang, L. Li, L. Xu, X. Peng, and A. Fei, "Failure-resilient distributed inference with model compression over heterogeneous edge devices," *IEEE Transactions on Mobile Computing*, vol. 23, no. 12, pp. 12 680–12 692, 2024.
- [14] J. Yang, Y. Wang, H. Zhao, and G. Gui, "Mobilenet and knowledge distillation-based automatic scenario recognition method in vehicle-to-vehicle systems," *IEEE Transactions on Vehicular Technology*, vol. 71, no. 10, pp. 11 006–11 016, 2022.
- [15] F. Chollet, "Xception: Deep learning with depthwise separable convolutions," in *2017 IEEE Conference on Computer Vision and Pattern Recognition (CVPR)*, 2017, pp. 1800–1807.
- [16] X. Wei, W. Luo, X. Zhang, J. Yang, G. Gui, and T. Ohtsuki, "Differentiable architecture search-based automatic modulation classification," in *2021 IEEE Wireless Communications and Networking Conference (WCNC)*, 2021, pp. 1–6.
- [17] X. Zhang, H. Zhao, H. Zhu, B. Adebisi, G. Gui, H. Gacanin, and F. Adachi, "Nas-amr: Neural architecture search-based automatic modulation recognition for integrated sensing and communication systems," *IEEE Transactions on Cognitive Communications and Networking*, vol. 8, no. 3, pp. 1374–1386, 2022.
- [18] F. Zhang, C. Luo, J. Xu, and Y. Luo, "An efficient deep learning model for automatic modulation recognition based on parameter estimation and transformation," *IEEE Communications Letters*, vol. 25, no. 10, pp. 3287–3290, 2021.
- [19] Y. Tu and Y. Lin, "Deep neural network compression technique towards efficient digital signal modulation recognition in edge device," *IEEE Access*, vol. 7, pp. 58 113–58 119, 2019.
- [20] S. Tridgell, D. Bolland, P. H. Leong, and S. Siddhartha, "Real-time automatic modulation classification," in *2019 International Conference on Field-Programmable Technology (ICFPT)*, 2019, pp. 299–302.
- [21] M. Li, G. Liu, S. Li, and Y. Wu, "Radio classify generative adversarial networks: A semi-supervised method for modulation recognition," in *2018 IEEE 18th International Conference on Communication Technology (ICCT)*, 2018, pp. 669–672.
- [22] Y. Dong, X. Jiang, L. Cheng, and Q. Shi, "Srcnn: A semi-supervised learning framework for signal recognition," *IEEE Transactions on Cognitive Communications and Networking*, vol. 7, no. 3, pp. 780–789, 2021.
- [23] D. Liu, P. Wang, T. Wang, and T. Abdelzaher, "Self-contrastive learning based semi-supervised radio modulation classification," in *MILCOM 2021 - 2021 IEEE Military Communications Conference (MILCOM)*, 2021, pp. 777–782.
- [24] B. K. Iwana and S. Uchida, "An empirical survey of data augmentation for time series classification with neural networks," *CoRR*, vol. abs/2007.15951, 2020. [Online]. Available: <https://arxiv.org/abs/2007.15951>
- [25] T. Chen, S. Kornblith, M. Norouzi, and G. E. Hinton, "A simple framework for contrastive learning of visual representations," *CoRR*, vol. abs/2002.05709, 2020. [Online]. Available: <https://arxiv.org/abs/2002.05709>
- [26] Z. Wu, Y. Xiong, S. X. Yu, and D. Lin, "Unsupervised feature learning via non-parametric instance discrimination," in *2018 IEEE/CVF Conference on Computer Vision and Pattern Recognition*, 2018, pp. 3733–3742.
- [27] A. P. Hermawan, R. R. Ginanjar, D.-S. Kim, and J.-M. Lee, "Cnn-based automatic modulation classification for beyond 5g communications," *IEEE Communications Letters*, vol. 24, no. 5, pp. 1038–1041, 2020.
- [28] T. Huynh-The, C.-H. Hua, Q.-V. Pham, and D.-S. Kim, "Mcnnet: An efficient cnn architecture for robust automatic modulation classification," *IEEE Communications Letters*, vol. 24, no. 4, pp. 811–815, 2020.
- [29] J. Zhang, T. Wang, Z. Feng, and S. Yang, "Toward the automatic modulation classification with adaptive wavelet network," *IEEE Transactions on Cognitive Communications and Networking*, vol. 9, no. 3, pp. 549–563, 2023.
- [30] C. Xiao, S. Yang, and Z. Feng, "Complex-valued depthwise separable convolutional neural network for automatic modulation classification," *IEEE Transactions on Instrumentation and Measurement*, vol. 72, pp. 1–10, 2023.